J. Cent. South Univ. (2022) 29: 4002−4020
DOI: https://doi.org/10.1007/s11771-022-5207-2

Springer

Time-dependent behaviors and volumetric recovery phenomenon of sandstone under triaxial loading and unloading

SONG Zhi-xiang(宋治祥), ZHANG Jun-wen(张俊文)*, DONG Xu-kai(董续凯), ZHANG Yang(张杨), ZHANG Yu-jie(张玉杰), AN Sai(安赛)

School of Energy and Mining Engineering, China University of Mining and Technology (Beijing), Beijing 100083, China

© Central South University 2022

Abstract: The time-dependent behaviors of coal and rocks were easily ignored. Besides, "three-stage" triaxial loading and unloading mechanics tests of sandstone were conducted based on the idea of the initial high in-situ stress state recovery according to the full-life cycle evolution characteristics of surrounding rocks in deep mines (pre-excavation, excavation and post-excavation). The time-dependent stress−strain curves of sandstone were obtained. Meanwhile, the deformation and strength fitting relationships with time of sandstone were also built. Furthermore, the dilatancy and volumetric recovery mechanical mechanisms of sandstone were revealed. The results showed that: 1) There were significant time-dependent evolution characteristics on the deformation and strength of sandstone; 2) There were significant correlations among the internal friction angle, cohesion and the simulated depths; 3) Volumetric recovery phenomenon of sandstone was observed for the first time, which mainly occurred at the simulated depth of 2000 m. The above research conclusions could provide a certain theoretical basis for the stability control of surrounding rocks in deep mines.

Key words: initial high in-situ stress state; sandstone; time-dependent behaviors; depth effect; volumetric recovery

Cite this article as: SONG Zhi-xiang, ZHANG Jun-wen, DONG Xu-kai, ZHANG Yang, ZHANG Yu-jie, AN Sai. Time-dependent behaviors and volumetric recovery phenomenon of sandstone under triaxial loading and unloading [J]. Journal of Central South University, 2022, 29(12): 4002−4020. DOI: https://doi.org/10.1007/s11771-022-5207-2.

1 Introduction

With the exhaustion of shallow coal resources, the mining depths of coal mines in China would expect to gradually increase to 1000 − 1500 m, or even 2000 m in the next 20 years. Owing to the complex environment of deep mines, the mechanical behavior characteristics of high energy, large deformation, difficult maintenance and strong time-dependent are induced [1−6]. Sandstone is one of the most common engineering geological materials in coal mines [7 − 8]. Therefore, it is necessary to obtain the time-dependent behaviors of sandstone based on the initial high in-situ stress state recovery. Research conclusions can provide a certain of references for determining the reasonable supported time of surrounding rocks in deep mines. Currently, scholars have conducted extensive researches on the mechanics behaviors of coal and rocks, and obtained abundant achievements [9−15]. Specifically, ZHANG et al [16] conducted a series of triaxial tests of coal under various confining pressures corresponding to the buried depths of 300,

Foundation item: Projects(52034009, 51974319) supported by the National Natural Science Foundation of China; Project(2020JCB01) supported by the Yue Qi Distinguished Scholar Project of China
Received date: 2022-06-09; **Accepted date:** 2022-08-09
Corresponding author: ZHANG Jun-wen, PhD, Professor; Tel: +86-13681359725; E-mail: zhangjw@cumtb.edu.cn; ORCID: https://orcid.org/0000-0001-6226-1693

600, 700, 850 and 1050 m. And the time-dependent deformations, strength evolution characteristics, and energy competition mechanism of coal at different buried depths were obtained. Besides, YANG et al [17] conducted the indirect tensile and triaxial mechanical tests of deep marble with the buried depths of 1500 − 2000 m. Meanwhile, the micro-deformation mechanism of deep buried marble was characterized. Besides, GONG et al [18 − 19] conducted the true triaxial mechanical tests of granite with pre-set holes at simulated depths of 500 and 1000 m. Furthermore, the failure mechanism of granite with pre-set holes was revealed. ZHANG et al [20 − 23] conducted the true and traditional triaxial mechanical tests of sandstone with different confining pressures. Moreover, the strength and energy evolution mechanisms of sandstone at different simulated depths were obtained. ZHOU et al [24] performed a series of uniaxial, indirect tensile and triaxial mechanical tests of basalt with confining pressures at buried depths of 410 − 1010 m, and comprehensively studied the evolution characteristics of the basic mechanical parameters of basalt. Besides, some scholars also reported that the buried depth notably influenced the mechanical behaviors and mechanisms of coal and rocks, even rock bolts [25−33].

Additionally, Zhao [34] had clearly pointed out that it was still an un-solved problem to accurately predict the time, area and energy of the failure of rocks under simple conditions in terms of advanced monitoring and tracking technologies. It shows that there is a certain time effect whether the rocks are under short-term or long-term loading. If the critical prediction of short-term aging could be made for rocks, it would bring a certain theoretical basis and guidance for earthquake engineering. Besides, previous researchers [35 − 41] analyzed the critical slowing phenomena of multiple parameters of acoustic emission (AE), such as rise time divided by the maximum amplitude/average freqnency (RA/AF), electric potential (EP), duration and rise time. And the researchs could also provide a certain theoretical basis for identifying precursor information and predicting the time of rock failure. To sum up, accurately predicting the rock failure time was a key problem that needs to be solved in the future no matter under short-term or long-term loading, and the corresponding time effect should naturally be focused and further studied.

Nevertheless, some previous studies on the mechanics behaviors of coal and rocks were still limited to the mining depths of 800−1500 m, which could lead to many differences and blind spots in that of coal and rocks at buried depths of 1500 − 2000 m. And most scholars ignored the initial damage of coal and rocks in high in-situ stress before the tests. Sandstone was selected as the research object. A “three-stage” loading stress path was proposed based on the recovery of initial high in-situ stress state. The time-dependent behaviors of sandstone under triaxial loading and unloading were extensively investigated. Furthermore, the dilatancy and volumetric recovery mechanical mechanism under the new stress path were revealed.

2 Experimental methods

The multi-field coupling servo system was adopted to conduct the triaxial loading and unloading tests. Besides, the sandstone was extracted from the surrounding rocks of deep roadway with the depth of 1150 m in Suncun Coal Mine. The sandstone samples were processed to cylindrical specimens with the diameter of 25 mm and height of 50 mm.

The new stress path was proposed and designed according to the excavation process of the surrounding rocks in deep mines: before excavation (stage I: Recovery of initial high in-situ stress state) → excavation (stage II: constant axial pressure and unloading confining pressure) → after excavation (stage III: constant confining pressure and loading axial pressure). The loading or unloading control mode, loading or unloading rate, corresponding simulated depths, and the confining pressure sets for each stage of the specific tests were presented in Table 1. The engineering background and new stress path were shown in Figures 1 and 2, respectively.

The details and parameters of the triaxial loading and unloading tests were quoted from the following references [21−23].

3 Experimental results

3.1 Time-dependent stress−strain curves

As shown in Figure 3, the time pertaining to stage I of sandstone was nearly identical under the same simulated depth, indicating that the internal

Table 1 Parameters of "three-stage" stress path

Stress loading stage	Loading/ unloading model	Loading/ unloading rate	Simulated depth and corresponding stress value [42−45]
Stage I: Initial high in-situ stress state recovery	Stress control	Loading rate: 4 MPa/min	H=1000 m (σ_1: 0→27.0 MPa, σ_3: 0→23.0 MPa) H=1500 m (σ_1: 0→40.5 MPa, σ_3: 0→36.5 MPa) H=2000 m (σ_1: 0→54.0 MPa, σ_3: 0→50.0 MPa)
Stage II: Constant axial pressure-unloading confining pressure	Stress control	Unloading rate: 2 MPa/min	H=1000 m (σ_1=27.0 MPa, σ_3: 23.0 MPa→20.0 MPa, 13.0 MPa, 6.0 MPa) H=1500 m (σ_1=40.5 MPa, σ_3: 36.5 MPa→20.0 MPa, 13.0 MPa, 6.0 MPa) H=2000 m (σ_1=54.0 MPa, σ_3: 50.0 MPa→20.0 MPa, 13.0 MPa, 6.0 MPa)
Stage III: Constant confining pressure-loading axial pressure	Strain control	Loading rate: 0.05%/min	H=1000 m (σ_1=27.0 MPa ↑, σ_3=6.0 MPa, 13.0 MPa, 20.0 MPa) H=1500 m (σ_1=40.5 MPa ↑, σ_3=6.0 MPa, 13.0 MPa, 20.0 MPa) H=2000 m (σ_1=54.0 MPa ↑, σ_3=6.0 MPa, 13.0 MPa, 20.0 MPa)

Note: H is the simulated depth; σ_1 and σ_3 are the axial stress and confining pressure, respectively. The "→" in the stage I represents the loading process. And the loading process is that the axial stress, σ_1 and confining pressure σ_3 are both from 0 MPa loaded to 27 MPa and 23 MPa, 40.5 MPa and 36.5 MPa, 54 MPa and 50 MPa under different simulated depths of 1000 m, 1500 m, 2000 m with the loading rate of 4 MPa/min, respectively. The "→" in the stage II represents the unloading process. And the unloading process is that the confining pressure σ_3 are both from 23 MPa, 36.5 MPa, 50 MPa unloaded to 6 MPa , 13 MPa and 20 MPa with the unloading rate of 2 MPa/min under different simulated depths of 1000 m, 1500 m, 2000 m, respectively. The " ↑ " in the stage III represents the reloading process. And the reloading process is that the axial stress σ_1 from 27 MPa, 40.5 MPa, 54 MPa under different simulated depths of 1000 m, 1500 m, 2000 m are reloaded with the reloading rate of 0.05%/min, respectively, until the sandstone reached the residual deformation stage.

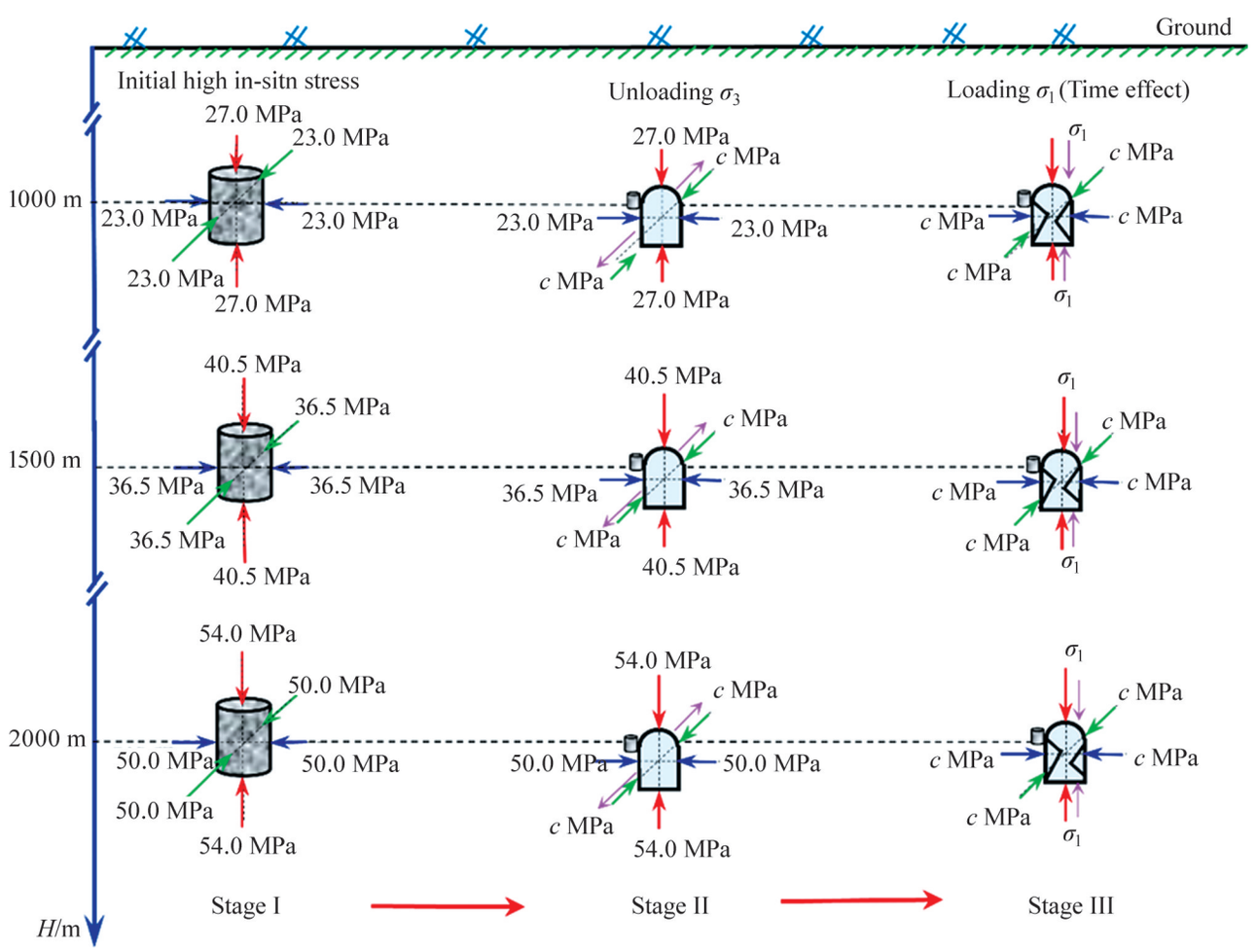

Figure 1 Engineering background (Note: H represents the simulation depth; σ_1 and σ_3 represent the axial stress and confining pressure, respectively; c represents the confining pressures of 6 MPa, 13 MPa and 20 MPa, corresponding to the gradient values of low, medium and high confining pressures, respectively)

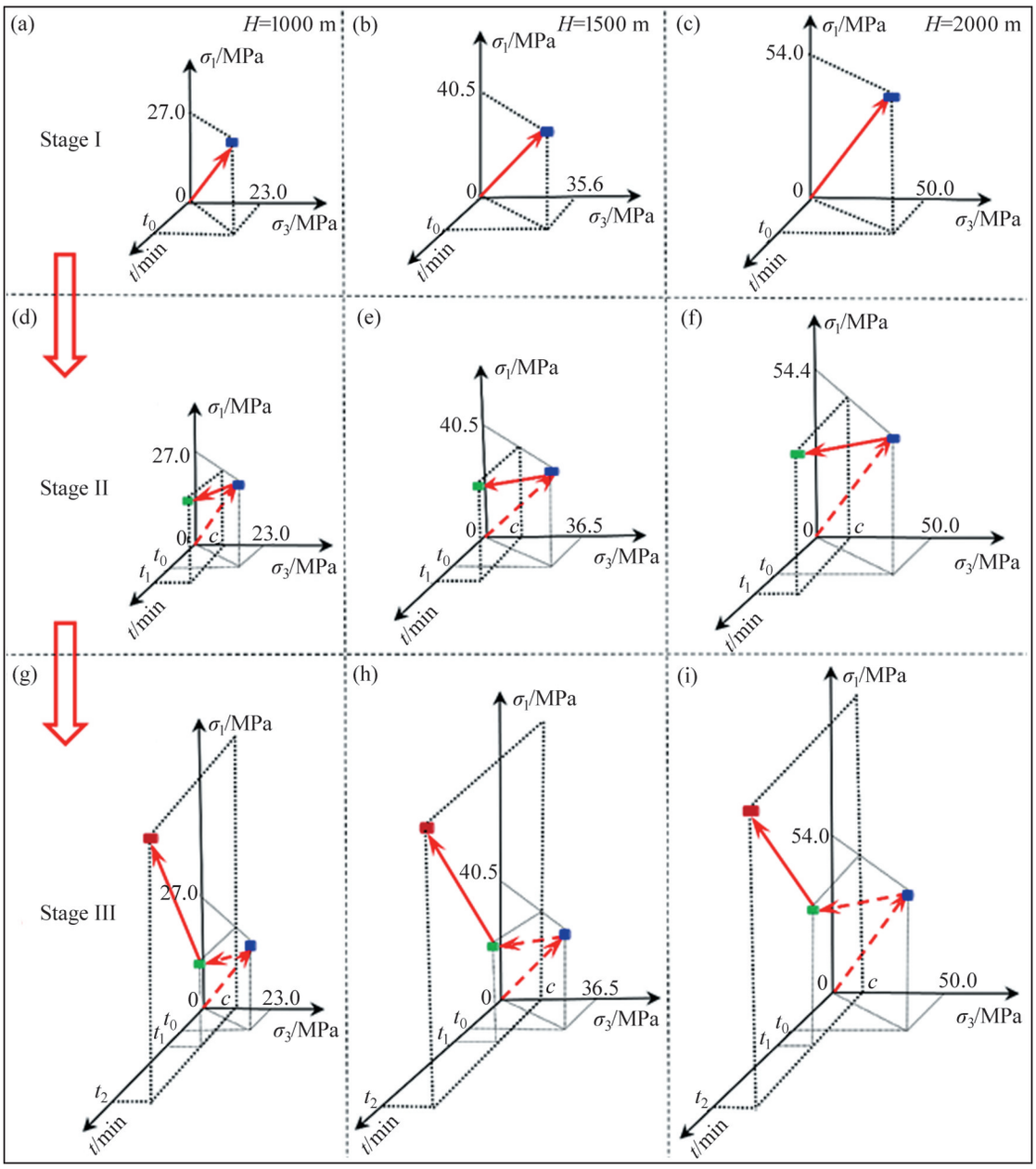

Figure 2 New stress path (Note: t_0, t_1 and t_2 represent the time of each stage, respectively; σ_1 and σ_3 are the axial stress and confining pressure, respectively; c represents the confining pressures of 6 MPa, 13 MPa and 20 MPa, corresponding to the gradient values of low, medium and high confining pressures, respectively)

compositions and spatial structures of sandstone were similar under the same simulated depth. Besides, the time for the whole deformation at the simulated depth of 2000 m was significantly longer than that at the simulated depths of 1000 m and 1500 m. The reason was that the recovery time in stage I of sandstone at a simulated depth of 2000 m was longer than that at the simulated depth of 1000 or 1500 m. Compared with the sandstone at the simulated depth of 1000 or 1500 m, the time-dependent characteristics of sandstone at the simulated depth of 2000 m were strengthened. The simulated depth corresponded to the axial pressure effect. Therefore, it was easy to make sandstone with a deeper simulated depth produce a larger deformation. Similarly, the whole life-cycle evolution process of roadway surrounding rocks in deep mines with corresponding buried depth could present its significant time-dependent characteristics. Besides, the time for the complete deformation of sandstone increased continuously with the increase of simulated depth under the same

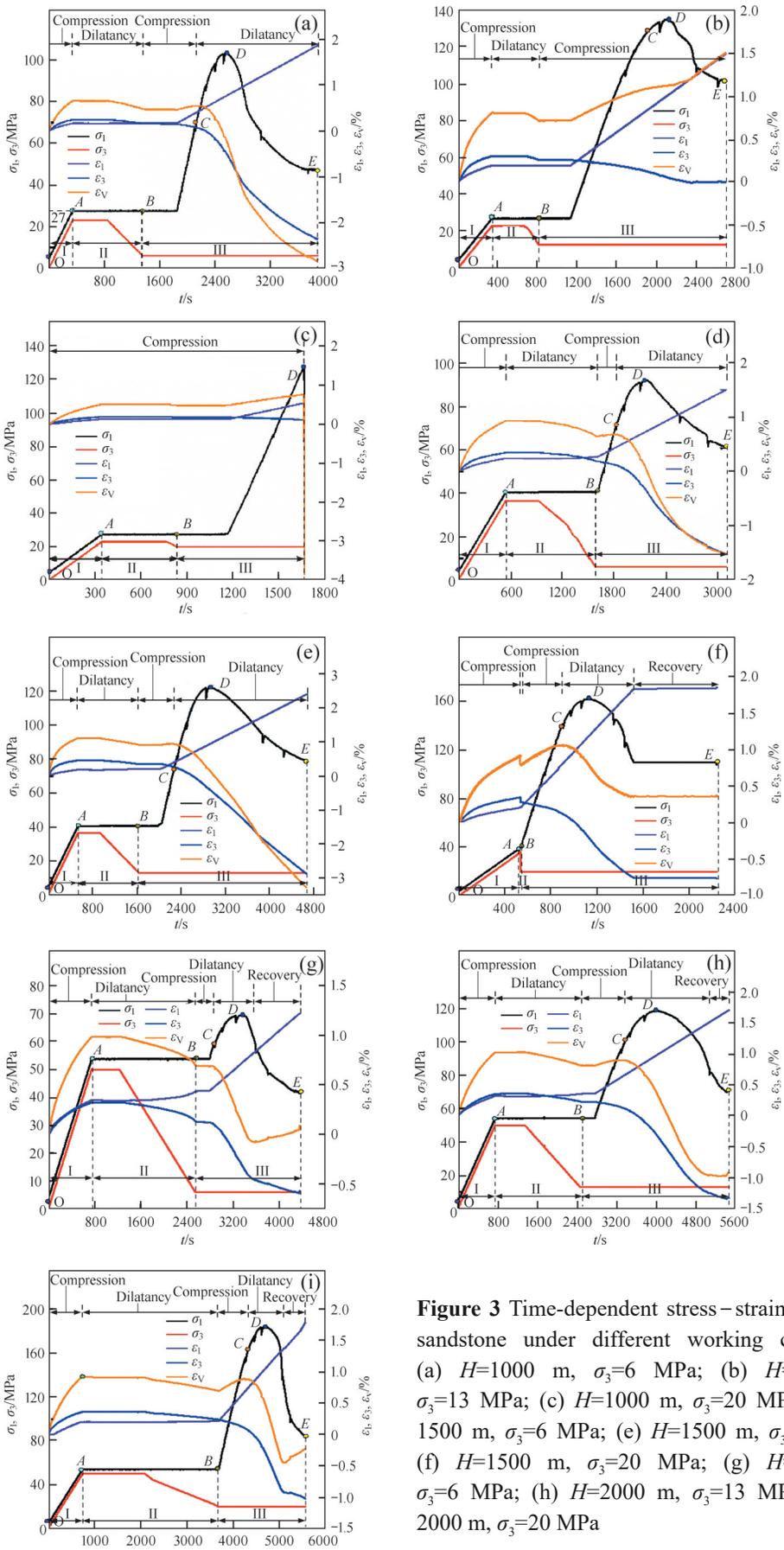

Figure 3 Time-dependent stress–strain curves of sandstone under different working conditions: (a) H=1000 m, σ_3=6 MPa; (b) H=1000 m, σ_3=13 MPa; (c) H=1000 m, σ_3=20 MPa; (d) H=1500 m, σ_3=6 MPa; (e) H=1500 m, σ_3=13 MPa; (f) H=1500 m, σ_3=20 MPa; (g) H=2000 m, σ_3=6 MPa; (h) H=2000 m, σ_3=13 MPa; (i) H=2000 m, σ_3=20 MPa

confining pressure, indicating that the depth effect could significantly enhance the time-dependent characteristics of sandstone (see Figure 3).

Moreover, the time-dependent stress−strain curves of sandstone under different working conditions exhibited the "three-stage" evolution characteristics with time changes due to the influence of the new stress path. Besides, the sandstone has complex deformations under different working conditions, including repeated changes in compression and expansion. Meanwhile, the dilatancy phenomenon and volumetric recovery characteristics were exhibited (see Figure 3). The analyses of the dilatancy and volumetric recovery characteristics were described in the section 3.4. Points *A* and *B* in Figure 3 were the cut-off points of stages I and II, stages II and III, respectively. Points *C*, *D* and *E* in Figure 3 were the thresholds of damage stress, peak stress and residual stress, respectively. The characteristics of stress thresholds are presented in Tables 2-4.

3.2 Time-dependent characteristies of stress−strain at different depths

3.2.1 Theoretical bases of crack initiation stress

Most scholars focused on the influences of the stress path, confining pressure, water, bedding, temperature, loading or unloading rate and other factors on the strength evolution characteristics of coal and rocks. Nevertheless, they both ignored the time-dependent behaviors of coal or rocks. The damage stress, peak stress, residual stress and their corresponding time could be determined according to the time-dependent stress − strain curves, but several scholars believed that the accurate identification about crack initiation stress of coal and rocks could provide a theoretical basis to realize early warnings of rock burst in deep mines.

There were several methods to determine the crack initiation stress of coal and rocks, including the methods of acoustic emission, crack volumetric strain, axial strain difference and so on. And the crack volumetric strain method was selected to

Table 2 Characteristics of damage stress

H/m	σ_3/MPa	σ_{1cd}/MPa	ε_{1cd}/%	ε_{Vcd}/%	t_{cd}/s
1000	6	70.1000	0.4027	0.5443	2138.9000
1000	13	133.5000	0.9432	1.1126	1921.5800
1000	20	—	—	—	—
1500	6	72.4000	0.4612	0.6843	1837.0600
1500	13	74.8000	0.4092	0.9410	2279.2800
1500	20	138.5300	0.7929	1.0623	897.7130
2000	6	59.4000	0.4929	0.6612	2879.2900
2000	13	101.9000	0.6085	0.9043	3387.9700
2000	20	163.1500	0.7466	0.8791	4325.9000

Note: ε_{1cd}, ε_{Ved} and t_{cd} represent the axial strain, volumetric strain and time corresponding to the damage stress, respectively.

Table 3 Characteristics of peak stress

H/m	σ_3/MPa	σ_{1cf}/MPa	ε_{1cf}/%	ε_{Vcf}/%	t_{cf}/s
1000	6	103.3000	0.7663	−0.2142	2592.8600
1000	13	134.9000	1.0051	1.1244	2135.5600
1000	20	127.6000	0.5391	0.7602	1666.3300
1500	6	92.3000	0.7279	0.0990	2155.0300
1500	13	122.2000	0.9525	0.1458	2933.2300
1500	20	161.8300	1.1975	0.7855	1135.7000
2000	6	69.5000	0.6649	0.2758	3371.2500
2000	13	118.8000	0.9922	0.3398	3981.9200
2000	20	183.8500	1.0519	0.4720	4695.8700

Note: ε_{1cf}, ε_{Vcf} and t_{cf} represent the axial, volumetric strains and time corresponding to the peak stress, respectively.

Table 4 Characteristics of residual stress

H/m	σ_3/MPa	σ_{1cr}/MPa	ε_{1cr}/%	ε_{Vcr}/%	t_{cr}/s
1000	6	47.7000	1.7743	−2.7546	3882.7600
1000	13	102.2000	1.4751	1.4848	2693.8600
1000	20	—	—	—	—
1500	6	60.7000	1.5112	−1.5175	3095.3200
1500	13	79.3000	2.3807	−3.2300	4669.2200
1500	20	109.7300	1.8375	0.3650	1520.5700
2000	6	43.3000	1.1287	0.0103	4351.0500
2000	13	70.4000	1.6949	−0.9345	5439.8100
2000	20	85.0500	1.7550	−0.2383	5545.1900

Note: ε_{1cr}, ε_{Vcr} and t_{cr} represent the axial, volumetric strains and time corresponding to the residual stress, respectively.

determine the initiation stress of sandstone due to the complexity of the loading stress path. Meanwhile, it was necessary to accurately determine the crack volumetric strain curves of sandstone under different working conditions to accurately determine the initiation stress of sandstone. Therefore, the following theoretical derivations were performed:

The volumetric strain of sandstone under the “three-stage” loading can be expressed as:

$$\varepsilon_V = \varepsilon_1 + 2\varepsilon_3 \tag{1}$$

Besides, the volumetric strain can be also expressed as:

$$\varepsilon_V = \varepsilon_V^e + \varepsilon_V^p \tag{2}$$

The axial and radial strains of sandstone under “three-stage” loading can be expressed as:

$$\begin{cases} \varepsilon_1 = \varepsilon_1^e + \varepsilon_1^p \\ \varepsilon_3 = \varepsilon_3^e + \varepsilon_3^p \end{cases} \tag{3}$$

According to the generalized Hooke’s law [39], the elastic axial and radial strains of sandstone under “three-stage” loading can be expressed as:

$$\begin{cases} \varepsilon_1^e = (\sigma_1 - 2\mu\sigma_3)/E \\ \varepsilon_3^e = [(1-\mu)\sigma_3 - \mu\sigma_1]/E \end{cases} \tag{4}$$

Combining Eqs. (3) and (4), the plastic axial and radial strains of sandstone under “three-stage” loading can be expressed as:

$$\begin{cases} \varepsilon_1^p = \varepsilon_1 - (\sigma_1 - 2\mu\sigma_3)/E \\ \varepsilon_3^p = \varepsilon_3 - [\sigma_3 - \mu(\sigma_1 + \sigma_3)]/E \end{cases} \tag{5}$$

Moreover, according to Eq. (5), the elastic volumetric strain of sandstone under “three-stage” loading can be expressed as:

$$\varepsilon_V^e = \varepsilon_1^e + 2\varepsilon_3^e = (1-2\mu)(\sigma_1 + 2\sigma_3)/E \tag{6}$$

Combining Eqs. (2), (3), (5) and (6), the crack volumetric strain of sandstone under "three-stage" loading can be expressed as:

$$\varepsilon_V^p = \varepsilon_V - \varepsilon_V^e = \varepsilon_V - (1-2\mu)(\sigma_1 + 2\sigma_3)/E \tag{7}$$

In the above Eqs. (1)−(7), ε_1, ε_3 and ε_V are the axial strain, radial strain and volumetric strain of sandstone, respectively; ε_V^e and ε_V^p are the elastic volumetric strain and crack volumetric strain of sandstone, respectively; ε_1^e and ε_1^p are the elastic axial strain and plastic axial strain of sandstone, respectively; ε_3^e and ε_3^p are the elastic radial strain and plastic radial strain of sandstone, respectively; σ_3 is the confining pressure, E and μ are the elastic modulus and Poisson ratio of sandstone, respectively.

The crack volumetric strain curves of sandstone at different simulated depths are shown in Figure 4. Therefore, the crack initiation stress and the corresponding axial, radial and volumetric strain of sandstone under different conditions can be obtained. The characteristics of crack initiation stress are presented in Table 5.

3.2.2 The relationship between characteristic stress and corresponding volumetric strain

According to the above analyses, combined with Tables 2 − 5, the fitting relationships of crack initiation stress, damage stress, peak stress and residual stress and corresponding volumetric strain of sandstone under the depth effect, confining pressure effect and time coupling were established. The corresponding fitting relationships are presented in Figures 5−12. Among them, the fitting

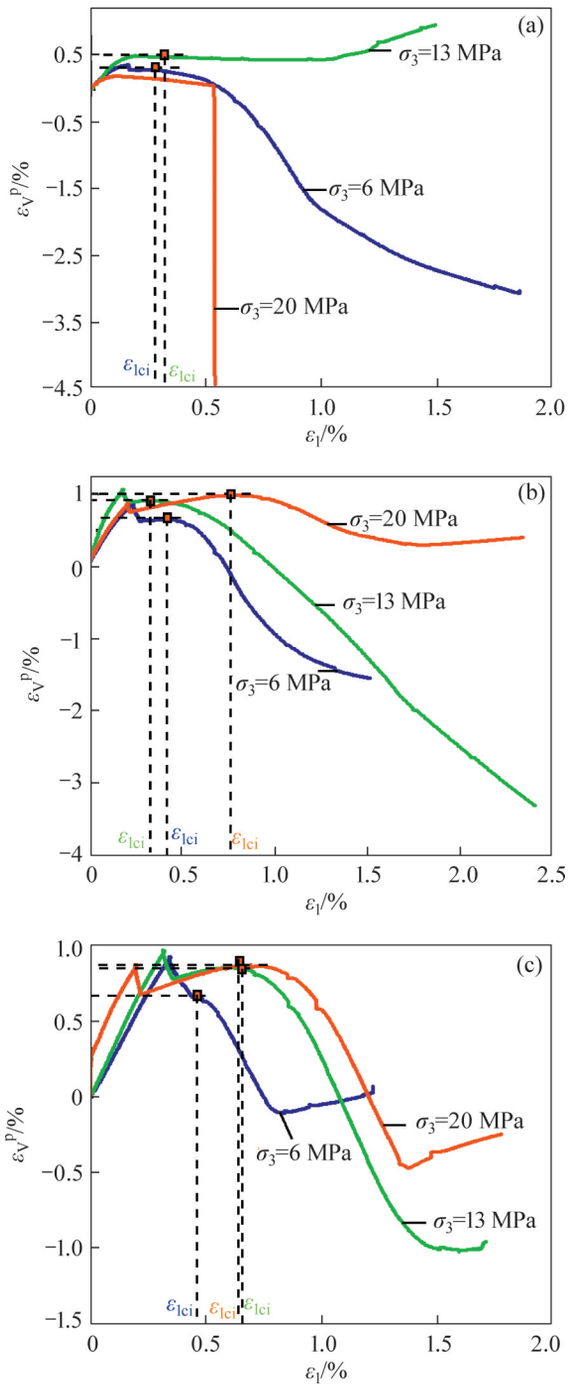

Figure 4 Crack volumetric strain curves of sandstone at different simulated depths: (a) H=1000 m; (b) H=1500 m; (c) H=2000 m

relationships were limited in the range of $H\in$[1000 m, 2000 m] or the range of $\sigma_3\in$[6 MPa, 20 MPa].

According to Figures 5−12, the fitting relationships of crack initiation stress, damage stress, peak stress and residual stress and corresponding volumetric strain of sandstone under the effects of confining pressure, depth effect and time coupling were the functions of binary quadric surfaces, respectively.

Besides, as shown in Figures 5 − 8, the crack

Table 5 Characteristics of the crack initiation stress

H/m	σ_3/MPa	σ_{1ci}/MPa	ε_{1ci}/%	ε_{Vci}/%	t_{ci}/s
1000	6	47.40	0.2744	0.5123	1982.91
1000	13	66.00	0.2956	0.6058	1385.62
1000	20	—	—	—	—
1500	6	65.70	0.4146	0.6862	1783.06
1500	13	62.20	0.3372	0.9456	2195.29
1500	20	129.23	0.7442	1.0507	856.726
2000	6	56.50	0.4578	0.6904	2831.29
2000	13	95.40	0.6221	0.9045	3283.98
2000	20	154.75	0.6120	0.8865	4255.90

Note: ε_{1ci}, ε_{Vci} and t_{ci} represent the axial, volumetric strains and time corresponding to the crack initiation stress, respectively.

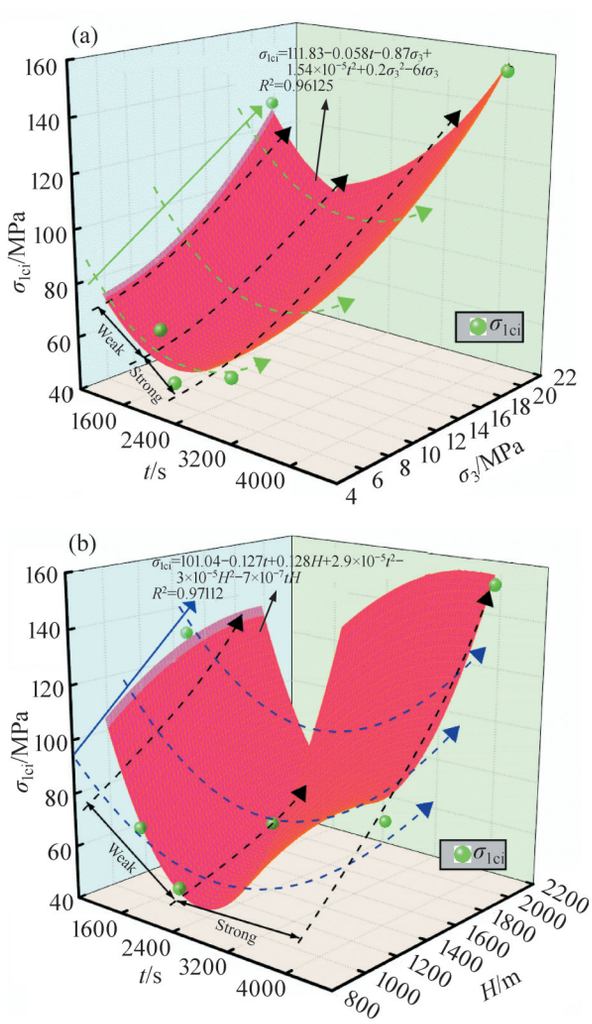

Figure 5 Fitting relationship of crack initiation stress: (a) Confining pressure and time; (b) Depth and time

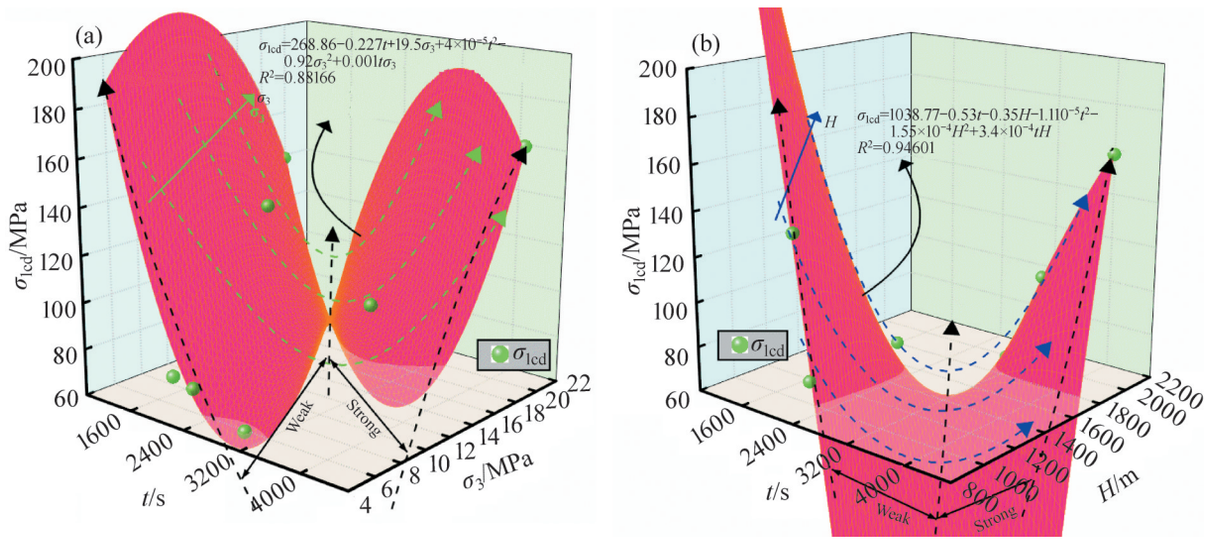

Figure 6 Fitting relationship of damage stress: (a) Confining pressure and time; (b) Depth and time

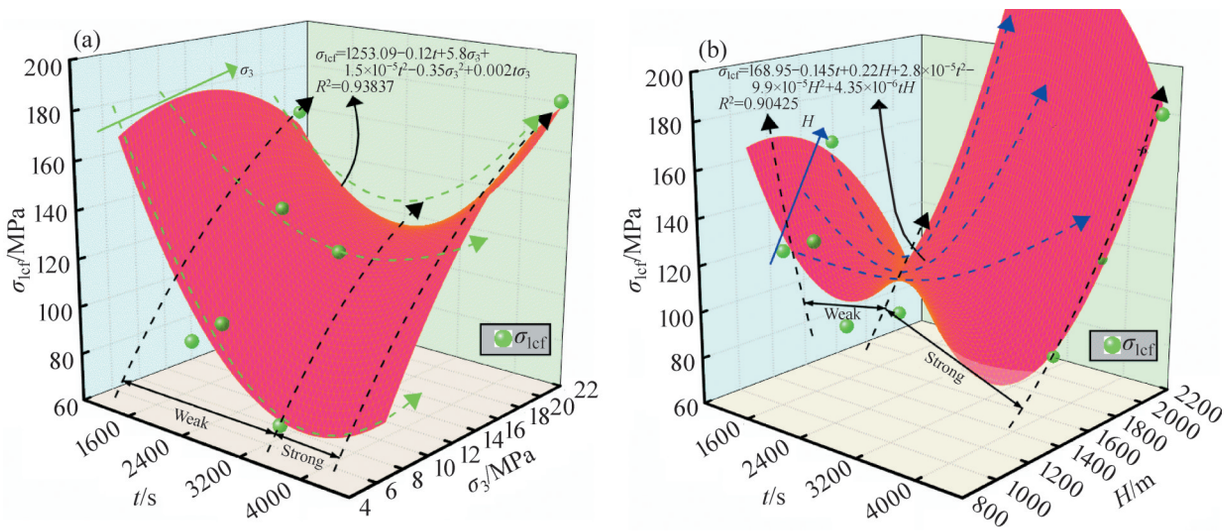

Figure 7 Fitting relationship of peak stress: (a) Confining pressure and time; (b) Depth and time

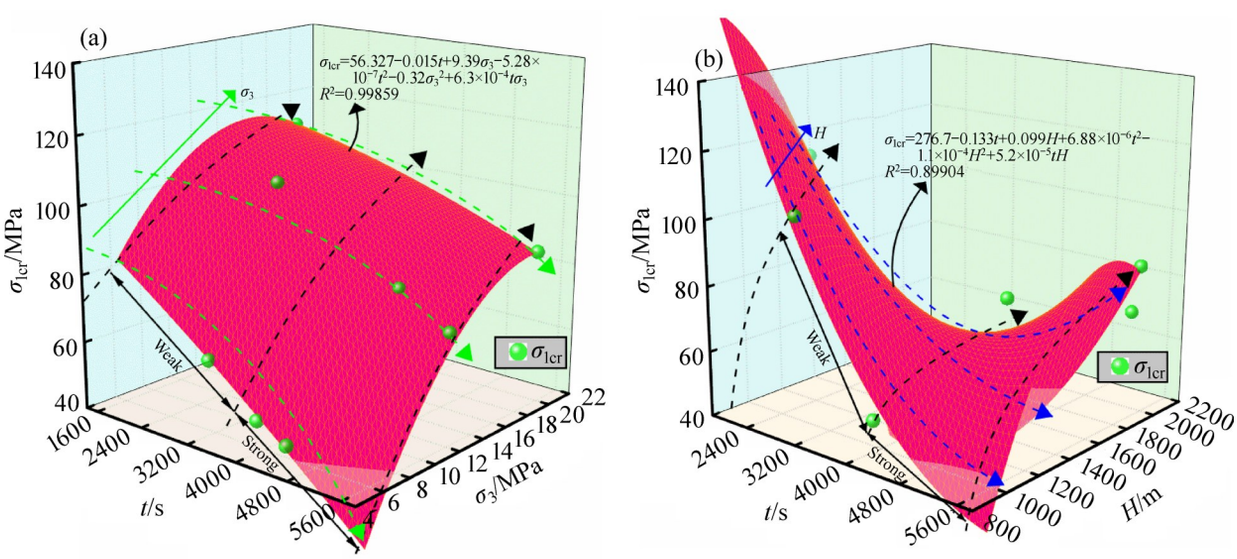

Figure 8 Fitting relationship of residual stress: (a) Confining pressure and time; (b) Depth and time

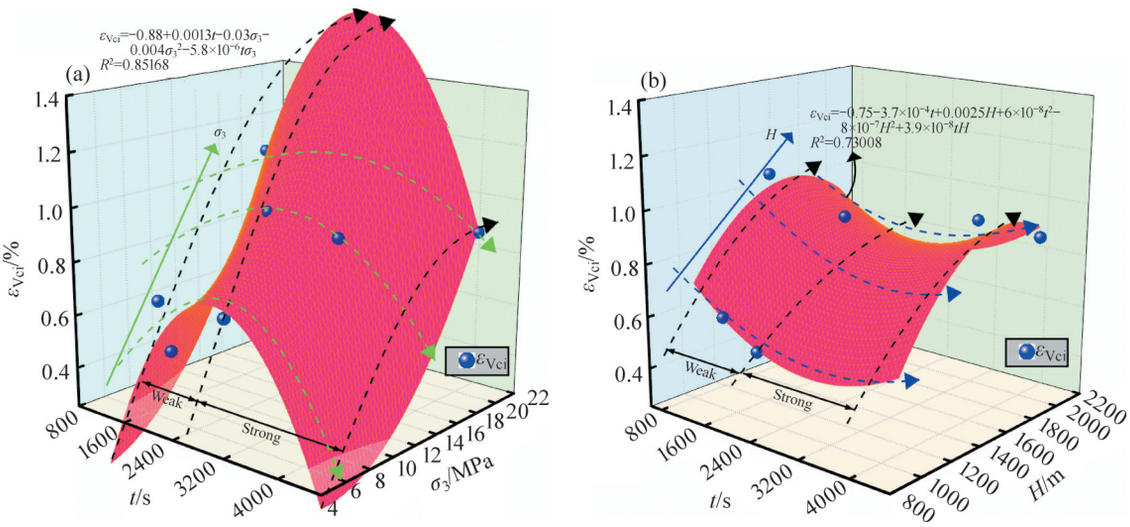

Figure 9 Fitting relationship of volumetric strain corresponding to the crack initiation stress: (a) Confining pressure and time; (b) Depth and time

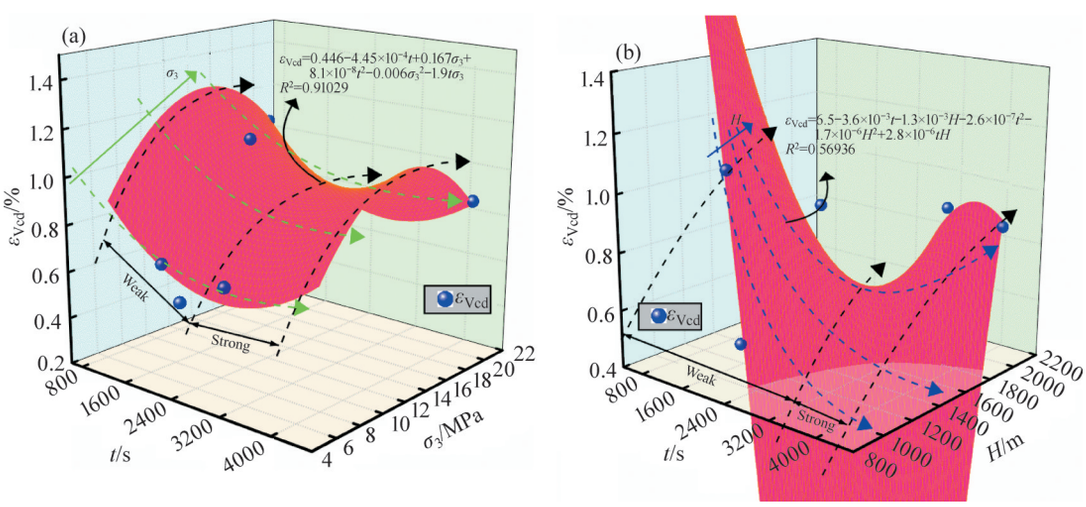

Figure 10 Fitting relationship of volumetric strain corresponding to the damage stress: (a) Confining pressure and time; (b) Depth and time

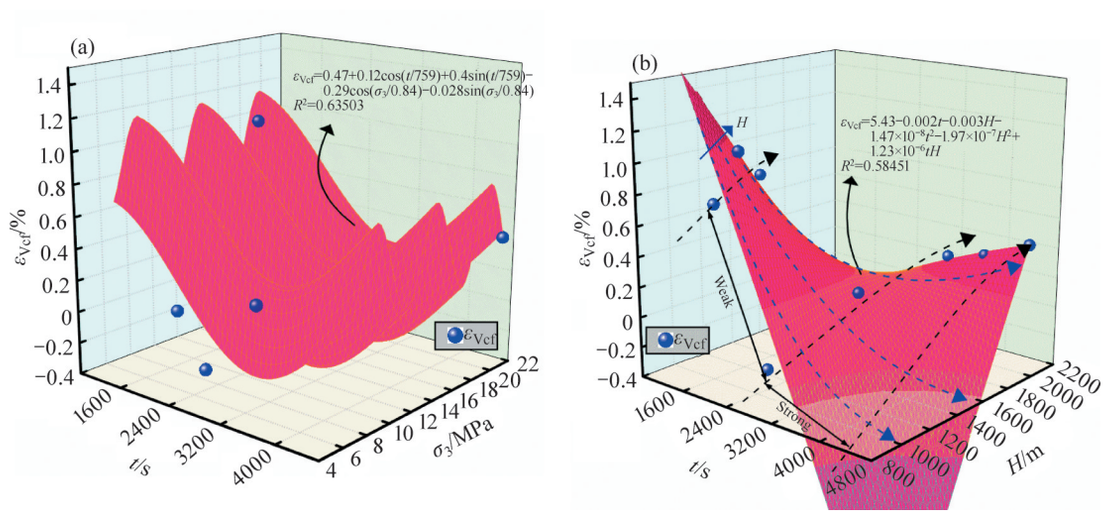

Figure 11 Fitting relationship of volumetric strain corresponding to the peak stress: (a) Confining pressure and time; (b) Depth and time

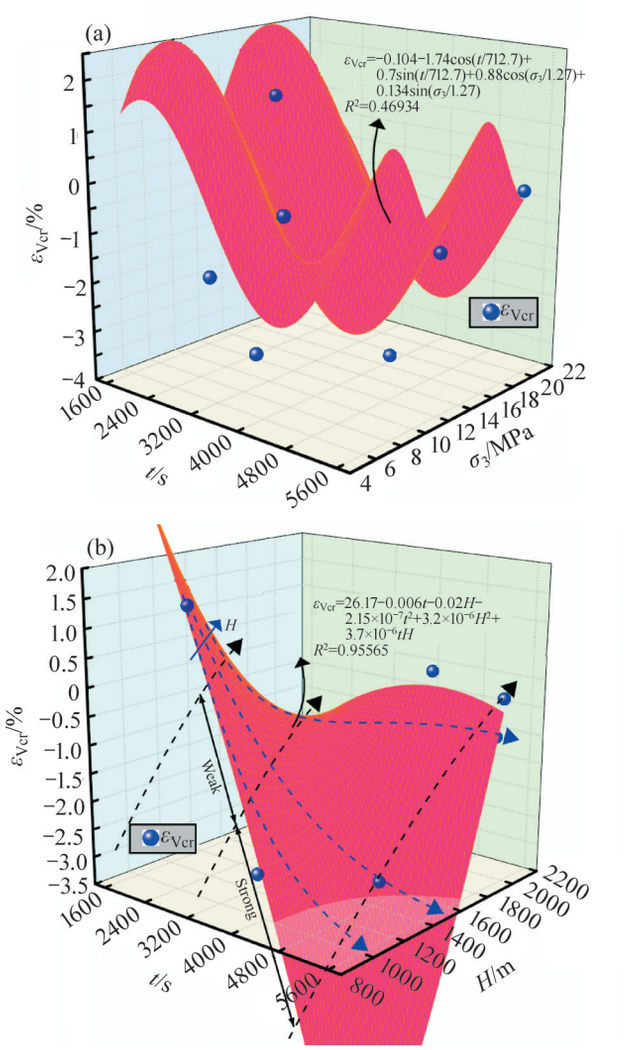

Figure 12 Fitting relationship of volumetric strain corresponding to the residual stress: (a) Confining pressure and time; (b) Depth and time

initiation stress, damage stress, peak stress and residual stress of sandstone under different simulated depths and confining pressures exhibited the significant time-dependent characteristics, which evolved from weak time-dependent to strong time-dependent. Each strength relationship exhibited a significant critical boundary in the whole deformation process. The crack initiation stress, damage stress and peak stress of sandstone under the same simulated depth and confining pressure decreased with time in the weak time-dependent range, while the opposite trends were observed with time in the strong time-dependent range. Additionally, despite the time-dependent ranges, the crack initiation stress, damage stress, peak stress and residual stress of sandstone at the same time increased with the increases of the simulated depth and confining pressure. Therefore, the effects of confining pressure and depth effect were significant. It was consistent with the characteristics that the bearing capacity of roadway surrounding rocks in deep mines decreased with the continuous extension of time. Then, it showed the obvious external characteristics of large deformation, difficult maintenance and strong time-dependent. It indicated that the time effect significantly affected the strength and bearing capacity of the roadway surrounding rocks in deep mines at different deformation stages.

As shown in Figures 9 – 12, the fitting correlation coefficients of the volumetric strain corresponding to the strength thresholds were not similarly to 1. Nevertheless, the evolution characteristics of the volumetric strain and strength were consistent. A significant correlation was observed between the volumetric strain evolution characteristics of sandstone and the time effect at different simulated depths and confining pressures. It indicated that the deformation and bearing capacity of the roadway surrounding rocks in deep mines were closely related to the time effect.

Therefore, the time effect of the surrounding rocks in deep roadway during the whole deformation process needs to be focused on. Besides, the evolution relationship of strength and corresponding volumetric strain of sandstone under the new stress path should be established because it could provide a certain reference for the stability control of surrounding rocks in deep mines.

3.3 The relationships amang the cohesion, internal friction angle and simulated depth

To further analyzed the deformation and failure mechanism of sandstone under the new stress path, the stress experienced by the sandstone in each deformation stage under different working conditions was extensively analyzed. Besides, the Mohr stress circle and its envelopes of sandstone corresponding to different stages were determined. And the basic strength parameters (cohesion and internal friction angle) of sandstone under the new stress path were obtained. The details are shown in Figure 13.

As shown in Figure 13, the Mohr stress circles of sandstone at different simulated depths exhibited

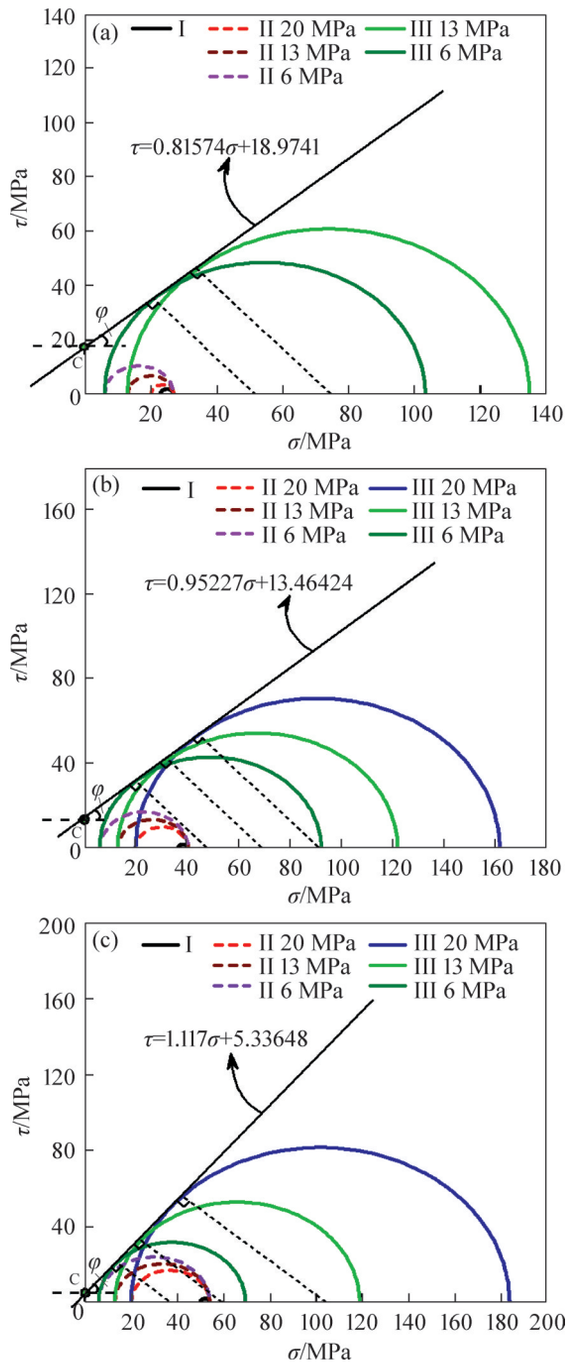

Figure 13 Mohr stress circle and its envelope of sandstone at different simulated depths: (a) H=1000 m; (b) H=1500 m; (c) H=2000 m

different degrees of lateral transition, which was closely related to "three-stage" stress path. In stage I, a constant deviatoric stress of 4 MPa was ensured to realize the recovery of initial high in-situ stress state of sandstone with hydrostatic pressure. Therefore, the radius of the Mohr stress circle of sandstone decreased, and the center of the Mohr stress circle was located far from the origin under different working conditions in stage I. In stage II, the axial stress remained constant with continuous unloading of the confining pressure. Therefore, the radius of the Mohr stress circle of sandstone increased, and the center of the Mohr stress circle approached the origin sequentially under different working conditions in stage II. A larger unloading amount of the confining pressure corresponded to the smaller radius of Mohr stress circle was; a larger deviation of the center of the circle from the origin occured. In stage III, the confining pressure was kept constant. Meanwhile, continuous loading of the axial pressure was applied on sandstone. Therefore, the radius of the Mohr stress circle of sandstone increased with the increase of the confining pressure. And the location of the center of the Mohr stress circle was located farther from the origin with the increase of the confining pressure under different working conditions. Besides, the internal friction angle (φ) and cohesion (C) of sandstone corresponding to different simulated depths are presented in Table 6.

Table 6 Cohesion and internal friction angle of sandstone under different simulated depths

H/m	C/MPa	φ/(°)
1000	18.97410	39.206
1500	13.46424	43.599
2000	5.33648	49.479

As shown in Table 6, the internal friction angle of sandstone increased with increasing the simulated depth. However, the cohesion of sandstone decreased with increasing the simulated depth, and the deep effect was significant.

As shown in Figure 14, the whole process of sandstone deformation can be divided into four stages. And the four stages were the elastic deformation (stage I), crack stable growth (stage II), crack unstable growth (stage III) and post-peak strain softening (stage IV), respectively. Additionally, relevant studies have shown that the whole deformation process of rocks under external loads was a cohesive-weakening-frictional-strengthening (CWFS) process [46-49]. And the CWFS model can reflect the gradual deformation evolution process of around underground engineering openings. In stage I , values of the cohesive strength and frictional strength were the

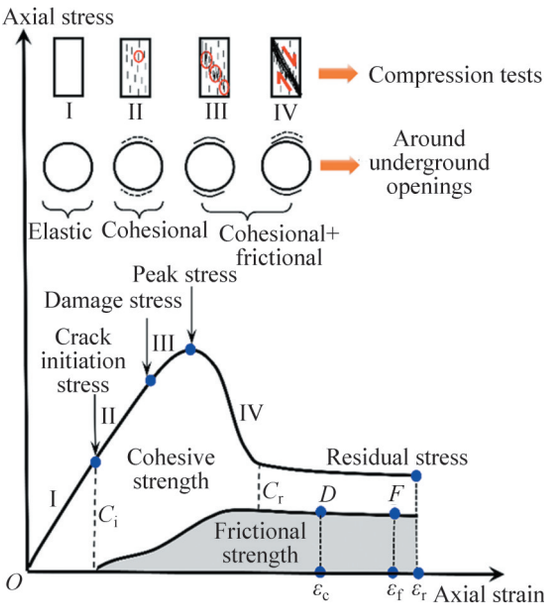

Figure 14 Relationship between CWFS model and field engineering application [46−49] (Note: C_i and C_r are the initial cohesion and residual cohesion, respectively; ε_c and ε_f are the plastic strains when the frictional strength and cohesive strength reached to the points *D* and *F*, which are the ultimate values of frictional strength and cohesive strength, respectively. ε_r is the residual axial strain corresponding to the residual stress)

value of initial cohesion and 0. In stage II, the cohesive strength and frictional strength were increased, but the increasing rate of cohesive strength was higher than frictional strength, which results in the cohesive strength of the around underground engineering openings in the stage II was dominant. However, in stages III and IV, the bearing capacity of around underground engineering openings was composed of the cohesive strength and frictional strength, but the frictional strength was dominant, and the reduced cohesion was transformed into residual cohesion.

Additionally, the simulated depth was corresponding to the initial state of high in-situ stress. The deeper the simulated depth was, the higher the corresponding initial high in-situ stress was. In addition, the unloading degree of the same confining pressure in the stage of constant axial pressure-unloading confining pressure was higher, which made the radial damage of sandstone severer, and the cohesion dropped faster with a deeper simulated depth of sandstone in equal time. Therefore, the cohesion decreased with the increases of the simulated depth.

Similarly, the internal friction angle corresponded to the internal friction strength. The larger the internal friction angle was, the severer the sandstone failure was, and the lower the cohesion bearing capacity was. The deeper the simulated depth was, the higher the degree of unloading the same confining pressure of the corresponding sandstone in stage II was, and the severer the radial damage of sandstone was in stage III. As a result, the internal friction angle increased with the increase of the simulated depth.

3.4 Dilatancy and volumetric recovery

The results indicated the volumetric strain of sandstone underwent a complex deformation process under different working conditions with the new stress path. Therefore, the dilatancy and volumetric recovery phenomena during the whole deformation process of sandstone under different working conditions need to be extensively analyzed (see Figure 15).

As shown in Figures 15(a) and (b), as the increase of the axial stress, the volume expansion and ductility expansion in stage III of volumetric strain curve of sandstone were observed (type ①). However, as shown in Figures 15(b) and (c), as the increase of the axial stress, the volume expansion and volume recovery after yielding in stage III of volumetric strain curve of sandstone were first observed (type ②). Among them, the starting point of volume recovery after yielding was called the volume recovery point. And as shown in Figure 15(a), there was no volume recovery point or expansion phenomenon in stage III of volumetric strain curve during the whole deformation process (type ③).

Additionally, the dilatancy onset and volumetric recovery onset of sandstone at different simulated depths occurred in prepeak and postpeak regions of the stress−strain curve respectively, and the details could be seen Table 7.

To further characterize the dilatancy and volumetric recovery phenomena, the data in Table 7 were reprocessed, and the corresponding data could be seen Table 8. Among them, the ratio of the damage stress to the peak strength, σ_{cd}/σ_{cf}, the ratio of the volumetric recovery stress to the peak

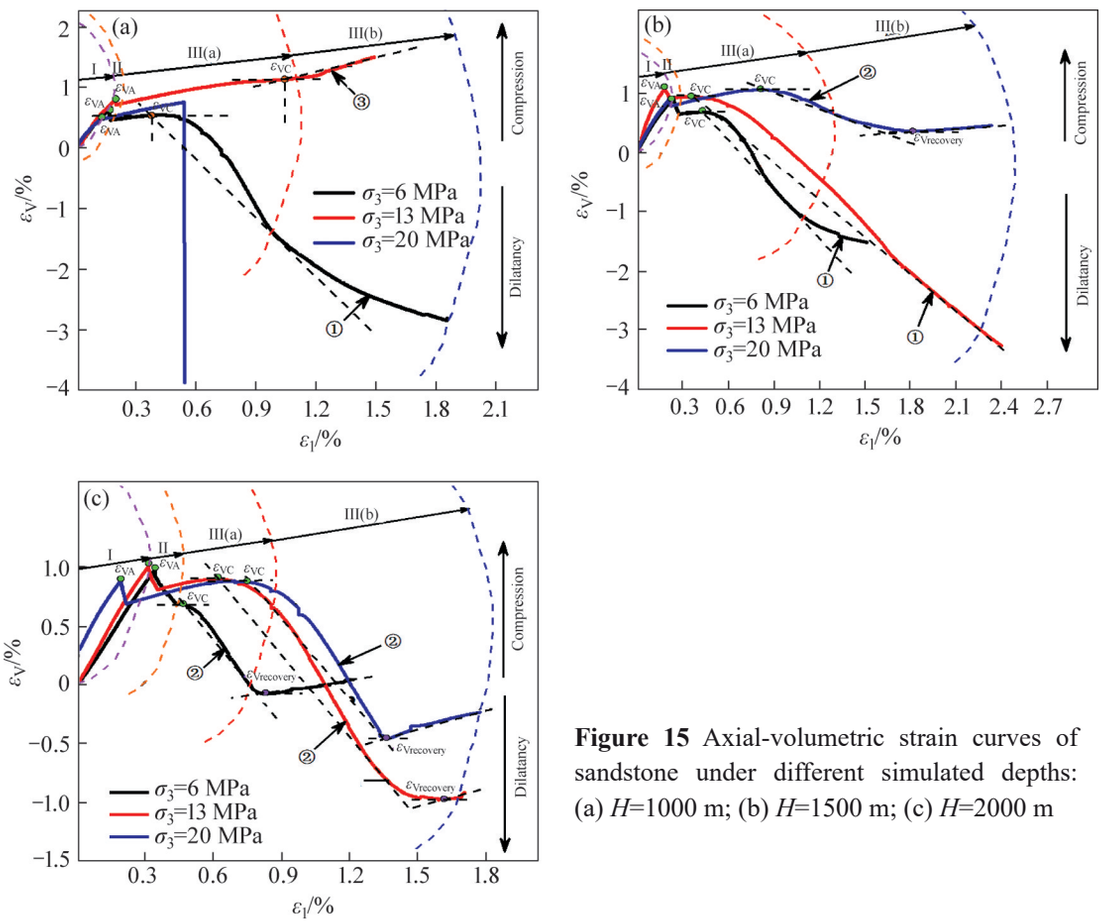

Figure 15 Axial-volumetric strain curves of sandstone under different simulated depths: (a) H=1000 m; (b) H=1500 m; (c) H=2000 m

Table 7 Dilatancy onset and volumetric recovery onset of volumetric strain curves at different working conditions

H/m	σ_3/MPa	σ_{cd}/MPa	ε_{VC}/%	t_{cd}/s	σ_{cg}/MPa	$\varepsilon_{Vrecovery}$/%	$t_{Vrecovery}$/s
1000	6	70.1000	0.5443	2138.9000	—	—	—
1000	13	—	—	—	—	—	—
1000	20	—	—	—	—	—	—
1500	6	72.4000	0.6843	1837.0600	—	—	—
1500	13	74.8000	0.9410	2279.2800	—	—	—
1500	20	138.5300	1.0623	897.7130	109.7300	0.3637	1521.5700
2000	6	59.4000	0.6612	2879.2900	62.0000	−0.0649	3559.2400
2000	13	101.9000	0.9043	3387.9700	84.7000	−0.9715	5055.8400
2000	20	163.1500	0.8791	4325.9000	138.2500	−0.4490	5069.8400

strength, σ_{cg}/σ_{cf}, and ratios of their corresponding time, t_{cd}/t_{cf}, t_{cg}/t_{cf}, were obtained.

According to the Table 8, the location of the volumetric recovery onset was at 67.8%−89.2% of that of the peak stress, and the taken time was 1.08−1.34 times the time required to attain the peak stress. And the location of the dilatancy onset was at 61.2%−88.7% of that of the peak stress, and the taken time was 77.7%−92.1% times the time required to attain the peak stress (see Table 8).

Additionally, to further analyzed the mechanical mechanism of the dilatancy and volumetric recovery of sandstone, the corresponding analyses were as follows (see Figure 16). Due to the recovery of initial high in-situ stress state in stage I, the axial and radial compression deformation of sandstone occurred in stage I (corresponding to Δh_1 and Δr_1, respectively, see Figure 16).

Table 8 The results of reprocessing data of dilatancy onset and volumetric recovery onset

H/m	σ_3/MPa	σ_{cd}/σ_{cf}	t_{cd}/t_{cf}	σ_{cg}/σ_{cf}	$t_{Vrecovery}/t_{cf}$
1000	6	0.679	0.825	—	—
1000	13	—	—	—	—
1000	20	—	—	—	—
1500	6	0.784	0.853	—	—
1500	13	0.612	0.777	—	—
1500	20	0.856	0.790	0.678	1.340
2000	6	0.855	0.854	0.892	1.056
2000	13	0.858	0.851	0.713	1.270
2000	20	0.887	0.921	0.752	1.080

Note: In Tables 7 and 8, H is the simulated depth; σ_3 is the confining pressure; σ_{cd}, σ_{cf}, and σ_{cg} denote the damage stress, peak stress and volumetric recovery stress corresponding to the volumetric recovery onset of sandstone under different working conditions, respectively; ε_{Vc}, t_{cd}, $\varepsilon_{Vrecovery}$ and $t_{Vrecovery}$ represent the volumetric strain and time corresponding to the dilatancy onset and volumetric recovery onset, respectively.

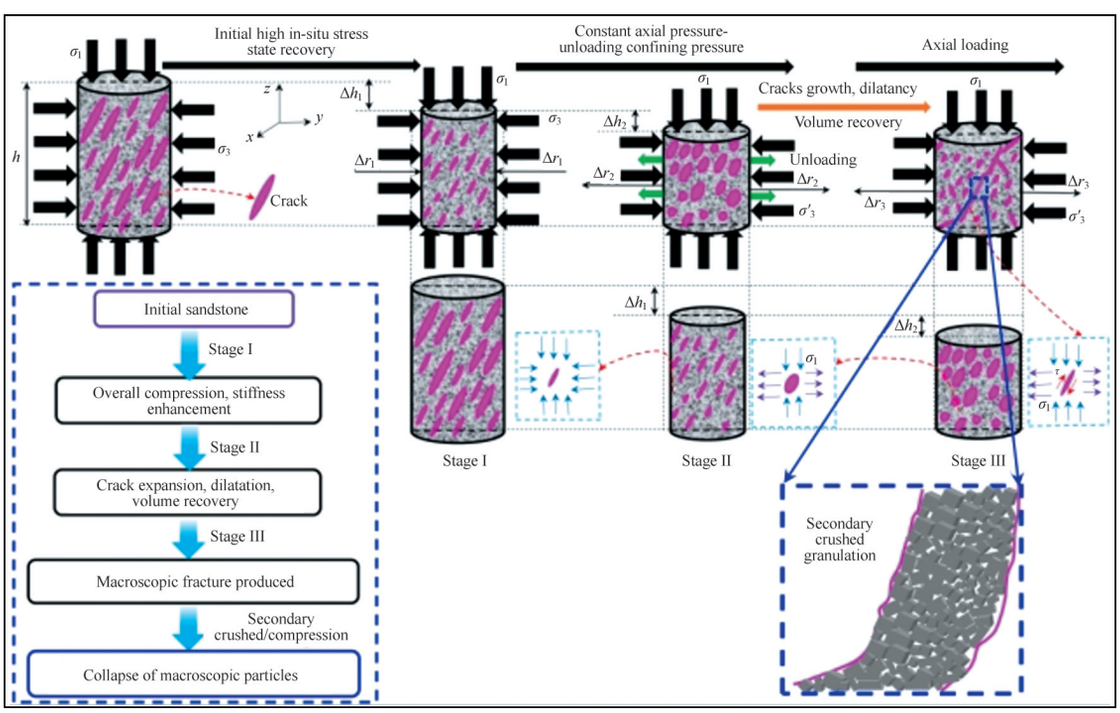

Figure 16 Mechanical mechanism of dilatancy and volumetric recovery of sandstone (Note: τ and σ_t represent the shear stress and tensile stress, respectively; h, σ_1 and σ_3 represent the initial height of sandstone, initial axial stress and initial confining pressure, respectively; σ_3 represent the confining pressure after unloading. Δh_1 and Δr_1 represent the axial compression deformation and radial compression deformation, respectively. Δh_2 and Δr_2 represent the axial compression deformation and radial expansion deformation, respectively. Δr_3 represents the radial deformation with first dilatancy then recovery or continuously dilatancy.)

Correspondingly, the numerous internal primary pores and cracks of sandstone were compacted closely. Therefore, it could result in the sandstone gradually transforming to a nearly rigid body. In stage II, with the constant axial pressure and unloading of the confining pressure to a certain value, the radial expansion deformation of sandstone occurred. And the notable axial compression phenomena (corresponding to Δh_2 and Δr_2, respectively, see Figure 16) were observed. According to the strength theory of Griffith, unloading the confining pressure weakened the radial inhibition effect in stage II. This caused the previously compacted cracks to re-open, and even

increases in the number and size (corresponding to the evolution characteristics of the internal cracks of sandstone, see Figure 16). Tensile stress developed around the cracks with increasing aperture. Then, the highly concentrated stress caused the axial deformation of sandstone. And it could lead to the axial compression and an increase in the axial strain.

After entering stage III, owing to the increased size of the internal pores and cracks of the sandstone, secondary compression occurred along with tensile extension, dislocation and nucleation. As shown in Figures 15 and 16, the dilatancy produced in the sandstone occurred owing to the enhanced reinforcement effect of axial loading in stage III (corresponding to Figure 16). And there are many new internal cracks and expanding growth occurrs under the sustained high axial stress loading after entering stage III(a). Besides, as shown in Figures 15 and 16, the volumetric strain curves of sandstone exhibited the characteristic of volumetric recovery after producing the dilatancy phenomenon at the simulated depth of 1500 m, confining pressure of 20 MPa, and simulated depth of 2000 m after entering stage III(b). Many collapsed particles were present in the macroscopic cracks produced in the sandstone, and the high confining pressure inhibited the outward expansion and extrusion of the collapsed particles in the macroscopic cracks. Furthermore, the continuous action of the axial loading would further compact the collapsed particles in the macroscopic cracks of sandstone, even leading to the secondary granulation of the collapsed particles in the macroscopic cracks of sandstone and it reduced the volume and space of the collapsed particles in the macroscopic cracks of sandstone. As a result, the volume of sandstone exhibited the notable volumetric recovery phenomenon.

4 Discussion

Considering the results of sandstone obtained in the “three-stage” triaxial loading and unloading mechanics tests, the time-dependent behaviors of sandstone were extensively analyzed under the new stress path. Meanwhile, the cohesion and internal friction angle of sandstone were obtained at different simulated depths. Nevertheless, the results and conclusions were preliminary due to the limited test data. Therefore, the following aspects need to be further emphasized and discussed.

First, compared with the conventional triaxial mechanical test, the “three-stage” stress path could more highly match the in-situ stress distribution characteristics of the roadway surrounding rocks in deep mines during the whole instability process from pre-excavation to post-excavation in terms of the evolution relationship between strength and corresponding volumetric strain. Furthermore, the evolution relationship between strength and volumetric strain considered the corresponding time at different strength thresholds. It could provide a certain reference to determine the reasonable supported time in deep mines. Besides, the data of experimental test obtained were limited, and the correlation coefficients were not close to 1. However, the concept of time could not only limit to the research on the rheological properties of coal and rocks, but also should gradually focused on the transforming to the non-rheological characteristics of the rock mechanics [50]. It could provide more valuable references and theoretical basis for the prevention, early warning and monitoring in deep mines.

Second, the cohesion and internal friction angle of sandstone were related to the depth effect. Therefore, on the research of deep rock mechanics, one should fully consider the characteristics of in-situ stress distribution of coal and rocks in different buried depth strata. And then the initial high in-situ stress state reduction before conducting the rock mechanical tests should be conducted. It could make the experimental conclusions reflect more accurately the deep engineering phenomena.

Third, the different types of volumetric strain curves of sandstone were obtained. Nevertheless, the evolution characteristics of volumetric strain at different simulated depths demonstrated that the phenomenon of volumetric recovery mainly occurred in the roadway with the depth of over 1000 m. Especially, sandstone at simulated depth of 2000 m was more likely to exhibit the phenomenon of volumetric recovery. The phenomenon could be primarily attributed to the effect of axial pressure. Meanwhile, the collapsed particles in the macroscopic cracks of sandstone produced

secondary granulation, which decreased the volume and space of the collapsed particles in the macroscopic cracks of sandstone.

5 Conclusions

Series of experiment have been conducted to study the strength evolution law and volumetric recovery phenomenon of sandstone. Based on the experimental results, some conclusions are given as follows:

1) The crack initiation stress, damage stress, peak stress and residual stress of sandstone at different simulated depths and confining pressures exhibited significant time-dependent evolution characteristics.

2) The internal friction angle of sandstone under the simulated depths of 1000, 1500 and 2000 m were 39.206°, 43.599° and 49.4793°, respectively, while the cohesions at different simulated depths were 18.97410, 13.46424 and 5.33648 MPa, respectively. With the increasing of simulated depth, the internal friction angle of sandstone increased, but the cohesion of sandstone decreased.

3) There were three types of volumetric strain curves of sandstone based on the idea of the initial high in-situ stress state recovery according to the full-life cycle evolution characteristics of surrounding rocks in deep mines (pre-excavation, excavation and post-excavation). Among them, as the increase of the axial stress, the volume expansion and ductility expansion in stage III of volumetric strain curves of sandstone were observed (type ①). However, as the increase of the axial stress, the volume expansion and volume recovery after yielding in stage III of volumetric strain curves of sandstone were first observed (type ②). Furthermore, the starting point of volume recovery after yielding was called the volume recovery point. Besides, there was no volume recovery point or expansion phenomenon in stage III of volumetric strain curve during the whole deformation process (type ③).

4) The dilatancy onset and volumetric recovery onset occurred in the pre peak and post peak regions of the stress–strain curve. Meanwhile, the location of the volumetric recovery onset was at 67.8%–89.2% of the peak strength, and the time taken was at 1.08–1.34 times the time required to attain the peak strength.

Contributors

SONG Zhi-xiang provided the concept, idea conducted the literature review, wrote the first draft of the manuscript and edited the draft of manuscript. ZHANG Jun-wen provided the supervision of manuscript, gave the funding acquisition and provided the resources for the manuscript. DONG Xu-kai, ZHANG Yang, ZHANG Yu-jie and AN Sai provided the re-supervision of manuscript.

Conflict of interest

The authors declare that they have no conflict of interest.

References

[1] YU Cheng-bo, JI Shao-cheng, LI Qi. Effects of porosity on seismic velocities, elastic moduli and Poisson's ratios of solid materials and rocks [J]. Journal of Rock Mechanics and Geotechnical Engineering, 2016, 8(1): 35–49. DOI: 10.1016/j.jrmge.2015.07.004.

[2] WANG Ming-yang, LI Jie, MA Lin-jian, et al. Study on the characteristic energy factor of the deep rock mass under weak disturbance [J]. Rock Mechanics and Rock Engineering, 2016, 49(8): 3165–3173. DOI: 10.1007/s00603-016-0968-2.

[3] WANG Gui-feng, GONG Si-yuan, LI Zhen-lei, et al. Evolution of stress concentration and energy release before rock bursts: Two case studies from Xingan coal mine, Hegang, China [J]. Rock Mechanics and Rock Engineering, 2016, 49(8): 3393–3401. DOI: 10.1007/s00603-015-0892-x.

[4] DUAN Shu-qian, FENG Xia-ting, JIANG Quan, et al. In situ observation of failure mechanisms controlled by rock masses with weak interlayer zones in large underground cavern excavations under high geostress [J]. Rock Mechanics and Rock Engineering, 2017, 50(9): 2465–2493. DOI: 10.1007/s00603-017-1249-4.

[5] LI Guo-qing, YAN De-tian, ZHUANG Xin-guo, et al. Implications of the pore pressure and in situ stress for the coalbed methane exploration in the southern Junggar Basin, China [J]. Engineering Geology, 2019, 262: 105305. DOI: 10.1016/j.enggeo.2019.105305.

[6] WANG Chun-lai, HE Bin-bin, HOU Xiao-lin, et al. Stress–energy mechanism for rock failure evolution based on damage mechanics in hard rock [J]. Rock Mechanics and Rock Engineering, 2020, 53(3): 1021–1037. DOI: 10.1007/s00603-019-01953-y.

[7] SU Rong-hua, LIU Xiao-lin. Fracture failure characteristics of jointed sandstone under uniaxial compression [J]. Geofluids, 2020: 8812522. DOI: 10.1155/2020/8812522.

[8] MARUVANCHERY V, KIM E. Effects of a high temperature

(500 ℃) on the fracture processes in calcite-cemented sandstone along bedding-plane orientations [J]. Rock Mechanics and Rock Engineering, 2020, 53(2): 955 − 966. DOI: 10.1007/s00603-019-01916-3.

[9] OLIVEIRA D A F, INDRARATNA B. Comparison between models of rock discontinuity strength and deformation [J]. Journal of Geotechnical and Geoenvironmental Engineering, 2010, 136(6): 864 − 874. DOI: 10.1061/(asce)gt.1943-5606.0000284.

[10] ISHII E, SANADA H, FUNAKI H, et al. The relationships among brittleness, deformation behavior, and transport properties in mudstones: An example from the Horonobe Underground Research Laboratory, Japan [J]. Journal of Geophysical Research Atmospheres, 2011, 116(B9): B09206. DOI: 10.1029/2011jb008279.

[11] ZHANG Rui, JIANG Zhen-quan, SUN Qiang, et al. The relationship between the deformation mechanism and permeability on brittle rock [J]. Natural Hazards, 2013, 66(2): 1179−1187. DOI: 10.1007/s11069-012-0543-4.

[12] WANG Shu-gang, ELSWORTH D, LIU Ji-shan. Mechanical behavior of methane infiltrated coal: The roles of gas desorption, stress level and loading rate [J]. Rock Mechanics and Rock Engineering, 2013, 46(5): 945−958. DOI: 10.1007/s00603-012-0324-0.

[13] WALTON G, ARZÚA J, ALEJANO L R, et al. A laboratory-testing-based study on the strength, deformability, and dilatancy of carbonate rocks at low confinement [J]. Rock Mechanics and Rock Engineering, 2015, 48(3): 941 − 958. DOI: 10.1007/s00603-014-0631-8.

[14] GHIRIAN A, FALL M. Strength evolution and deformation behaviour of cemented paste backfill at early ages: Effect of curing stress, filling strategy and drainage [J]. International Journal of Mining Science and Technology, 2016, 26(5): 809−817. DOI: 10.1016/j.ijmst.2016.05.039.

[15] WU Jing-ke, DONG Yun, JIANG Yang, et al. Research on plastic zone evolution law of surrounding rock of gob-side entry retaining under typical roof conditions in deep mine [J]. Shock and Vibration, 2020, 2020: 8864991. DOI: 10.1155/2020/8864991.

[16] ZHANG Zhao-peng, XIE He-ping, ZHANG Ru, et al. Deformation damage and energy evolution characteristics of coal at different depths [J]. Rock Mechanics and Rock Engineering, 2019, 52(5): 1491−1503. DOI: 10.1007/s00603-018-1555-5.

[17] YANG Sheng-qi, JU Yang, GAO Feng, et al. Strength, deformability and X-ray micro-CT observations of deeply buried marble under different confining pressures [J]. Rock Mechanics and Rock Engineering, 2016, 49(11): 4227−4244. DOI: 10.1007/s00603-016-1040-y.

[18] GONG Feng-qiang, LUO Yong, LI Xi-bing, et al. Experimental simulation investigation on rockburst induced by spalling failure in deep circular tunnels [J]. Tunnelling and Underground Space Technology, 2018, 81: 413 − 427. DOI: 10.1016/j.tust.2018.07.035.

[19] GONG Feng-qiang, SI Xue-feng, LI Xi-bing, et al. Experimental investigation of strain rockburst in circular Caverns under deep three-dimensional high-stress conditions [J]. Rock Mechanics and Rock Engineering, 2019, 52(5): 1459−1474. DOI: 10.1007/s00603-018-1660-5.

[20] ZHANG Jun-wen, SONG Zhi-xiang, FAN Wen-bing, et al. Experimental investigation on progressive damage mechanical behavior of sandstone under true triaxial condition [J]. Journal of China Coal Society, 2019, 44(9): 2700−2709. DOI: 10.13225/j.cnki.jccs.2019.0635. (in Chinese)

[21] ZHANG Jun-wen, SONG Zhi-xiang. Mechanical response and failure characteristics of deep sandstone under triaxial loading and unloading [J]. Journal of Mining & Safety Engineering, 2020(2): 409−418, 428. (in Chinese)

[22] ZHANG Jun-wen, SONG Zhi-xiang, WANG Shan-yong. Experimental investigation on permeability and energy evolution characteristics of deep sandstone along a three-stage loading path [J]. Bulletin of Engineering Geology and the Environment, 2021, 80(2): 1571 − 1584. DOI: 10.1007/s10064-020-01978-6.

[23] ZHANG Jun-wen, SONG Zhi-xiang, WANG Shan-yong. Mechanical behavior of deep sandstone under high stress-seepage coupling [J]. Journal of Central South University, 2021, 28(10): 3190−3206. DOI: 10.1007/s11771-021-4791-x.

[24] ZHOU Hong-wei, XIE He-ping, ZUO Jian-ping, et al. Experimental study of the effect of depth on mechanical parameters of rock [J]. Chinese Science Bulletin, 2010(34): 3276−3284. DOI: 10.1360/972010-786. (in Chinese)

[25] PATERSON M S. Experimental deformation and faulting in wombeyan marble [J]. Geological Society of America Bulletin, 1958, 69(4): 465. DOI: 10.1130/0016-7606(1958)69[465: edafiw]2.0.co;2.

[26] PATERSON M, WONG T. Experimental rock deformation: The brittle field [M]. 2nd ed. Springer, 2005. DOI: 10.1007/978-3-662-11720-0

[27] MAN Ke. Depth effect on dynamic fracture toughness of rock [J]. Metal Mine, 2011(3): 19−21. (in Chinese)

[28] VIOLAY M, GIBERT B, MAINPRICE D, et al. An experimental study of the brittle-ductile transition of basalt at oceanic crust pressure and temperature conditions [J]. Journal of Geophysical Research: Solid Earth, 2012, 117(B3). DOI: 10.1029/2011jb008884.

[29] ZUO Jian-ping, CHAI Neng-bin, ZHOU Hong-wei. Investigation on failure behavior of basalt from different depths based on three-point bending meso-experiments [J]. Chinese Journal of Rock Mechanics and Engineering, 2013, 32(4): 689−695.

[30] KAISER P K, KIM B H. Characterization of strength of intact brittle rock considering confinement-dependent failure processes [J]. Rock Mechanics and Rock Engineering, 2015, 48(1): 107−119. DOI: 10.1007/s00603-014-0545-5.

[31] WANG Yun-fei, ZHENG Xiao-juan, JIAO Hua-zhe, et al. Energy evolution mechanism and energy yield criterion in granite's failure process [J]. Explosion and Shock Waves, 2016c, 36(06): 876−882. DOI: 10.11883/1001-1455(2016)06-0876-07. (in Chinese)

[32] CHEN Jian-hang, LIU Peng, ZHAO Hong-bao, et al. Analytical studying the axial performance of fully encapsulated rock bolts [J]. Engineering Failure Analysis, 2021, 128: 105580. DOI: 10.1016/j.engfailanal.2021.105580.

[33] CHEN Jian-hang, LIU Peng, LIU Lei, et al. Anchorage performance of a modified cable anchor subjected to different joint opening conditions [J]. Construction and Building Materials, 2022, 336: 127558. DOI: 10.1016/j.conbuildmat.2022.127558.

[34] ZHAO Yang-sheng. Retrospection on the development of

rock mass mechanics and the summary of some unsolved centennial problems [J]. Chinese Journal of Rock Mechanics and Engineering, 2021(7): 1297−1336. (in Chinese)
[35] ZHU Xing, TANG Yao, FAN Jie, et al. Experimental study on failure precursors of fine sandstone based on critical slowing down theory [J]. Chinese Journal of Rock Mechanics and Engineering, 2022(1): 53−61. (in Chinese)
[36] ZHANG Zheng-hu, LI Ying-chun, HU Li-hua, et al. Predicting rock failure with the critical slowing down theory [J]. Engineering Geology, 2021, 280: 105960. DOI: 10.1016/j.enggeo.2020.105960.
[37] ZHANG Xin, LI Zhong-hui, NIU Yue, et al. An experimental study on the precursory characteristics of EP before sandstone failure based on critical slowing down [J]. Journal of Applied Geophysics, 2019, 170: 103818. DOI: 10.1016/j.jappgeo.2019.103818.
[38] KONG Xiang-guo, WANG En-yuan, HU Shao-bin, et al. Critical slowing down on acoustic emission characteristics of coal containing methane [J]. Journal of Natural Gas Science and Engineering, 2015, 24: 156−165. DOI: 10.1016/j.jngse.2015.03.020.
[39] WEI Yang, LI Zhong-hui, KONG Xiang-guo, et al. Critical slowing characteristics of sandstone under uniaxial compres-Sion failure [J]. Journal of China Coal Society, 2018, 43(2): 427−432. DOI: 10.13225/j.cnki.jccs.2017.0747. (in Chinese)
[40] WEI Yang, LI Zhong-hui, KONG Xiang-guo, et al. The precursory information of acoustic emission during sandstone loading based on critical slowing down theory [J]. Journal of Geophysics and Engineering, 2018, 15(5): 2150−2158. DOI: 10.1088/1742-2140/aac009.
[41] MATURANA M I, MEISEL C, DELL K, et al. Critical slowing down as a biomarker for seizure susceptibility [J]. Nature Communications, 2020, 11: 2172. DOI: 10.1038/s41467-020-15908-3.
[42] BROWN E T, HOEK E. Trends in relationships between measured in situ stresses and depth [J]. International Journal of Rock Mechanics and Mining Sciences & Geomechanics Abstracts, 1978, 15(4): 211−215. DOI: 10.1016/0148-9062(78)91227-5.
[43] LI Zhao-lin, WANG Lian-guo, LU Yin-long, et al. Experimental investigation on true triaxial deformation and progressive damage behaviour of sandstone [J]. Scientific Reports, 2019, 9: 3386. DOI: 10.1038/s41598-019-39816-9.
[44] KANG Hong-pu, YI Bing-ding, GAO Fu-qiang, et al. Database and characteristics of underground *in situ* stress distribution in Chinese coal mines [J]. Journal of China Coal Society, 2019, 44(1): 23 − 33. DOI: 10.13225/j.cnki.jccs.2018.5032. (in Chinese)
[45] FENG Yu, HARRISON J P, BOZORGZADEH N. Uncertainty in in situ stress estimations: A statistical simulation to study the effect of numbers of stress measurements [J]. Rock Mechanics and Rock Engineering, 2019, 52(12): 5071 − 5084. DOI: 10.1007/s00603-019-01891-9.
[46] GAO Fu-qiang, KANG Hong-pu. Experimental study on the residual strength of coal under low confinement [J]. Rock Mechanics and Rock Engineering, 2017, 50(2): 285 − 296. DOI: 10.1007/s00603-016-1120-z.
[47] HAJIABDOLMAJID V, KAISER P K, MARTIN C D. Modelling brittle failure of rock [J]. International Journal of Rock Mechanics and Mining Sciences, 2002, 39(6): 731 − 741. DOI: 10.1016/S1365-1609(02)00051-5.
[48] HUDSON J. Rock mechanics principles in engineering practice [M]. London: Butterworth-Heinemann, 1989. DOI: 10.1016/0148-9062(89)91449-6.
[49] RAFIEI RENANI H, MARTIN C D. Cohesion degradation and friction mobilization in brittle failure of rocks [J]. International Journal of Rock Mechanics and Mining Sciences, 2018, 106: 1 − 13. DOI: 10.1016/j.ijrmms.2018.04.003.
[50] KANG Hong-pu. Temporal scale analysis on coal mining and strata control technologies [J]. Journal of Mining and Strata Control Engineering, 2021, 3(1): 5 − 27. DOI: 10.13532/j.jmsce.cn10-1638/td.20200814.001.

(Edited by ZHANG Ou-ya)

中文导读

三轴加卸载下砂岩的时效行为及体积恢复

摘要：煤和岩石的时效力学行为往往很容易被忽略。为此，根据深部矿井围岩开挖前、开挖中和开挖后的全生命周期演化特征，基于初始高地应力状态恢复理论，对砂岩进行了“三阶段”三轴加卸载力学试验，获得了砂岩随时间变化的应力–应变曲线，构建了砂岩的变形和强度随时间的拟合关系，揭示了砂岩扩容和体积恢复的力学机制。结果表明：1)砂岩的变形与强度具有显著的时效演化特征；2)内摩擦角、内聚力与模拟深度具有显著的相关性；3)首次发现了砂岩的体积应变曲线出现“复容”现象，且该现象主要发生在模拟深度为2000 m处。上述研究结论可为深部矿井围岩稳定控制提供理论依据。

关键词：初始高地应力状态；砂岩；时效行为；深部效应；体积恢复